Hadronic vacuum polarization: three-pion channel

Bai-Long Hoid[1,a], Martin Hoferichter[2], and Bastian Kubis[1]

[1] *Helmholtz-Institut für Strahlen- und Kernphysik (Theorie) and Bethe Center for Theoretical Physics, Universität Bonn, 53115 Bonn, Germany*
[2] *Institute for Nuclear Theory, University of Washington, Seattle, WA 98195-1550, USA*

Abstract. The 3π-channel contribution to hadronic vacuum polarization (HVP) in the anomalous magnetic moment of the muon $(g-2)_\mu$ is examined based on a dispersive representation of the $\gamma^* \to 3\pi$ amplitude. This decay amplitude is reconstructed from dispersion relations, fulfilling the low-energy theorem of QCD. The global fit function is applied to the data sets of the 3π channel below 1.8 GeV, which constitutes the second-largest exclusive contribution to HVP and its uncertainty. The dominant ω- and ϕ-peak regions in the $e^+e^- \to 3\pi$ cross section as well as the non-resonant regions are precisely described to obtain our best estimate. The final result, $a_\mu^{3\pi}|_{\leq 1.8\,\mathrm{GeV}} = 46.2(6)(6) \times 10^{-10}$, reduces the model dependence owing to the fundamental principles of analyticity and unitarity and provides a cross check for the compatibility of the different $e^+e^- \to 3\pi$ data sets. A combination of the current analysis and the recent similar treatment of the 2π channel yields a dispersive determination of almost 80% of the entire HVP contribution. Our analysis reaffirms the muon anomaly at 3.4σ level, when the rest of the contributions is taken from the literature.

1 Introduction

A tantalizing discrepancy of 3–4 standard deviations between the experiment [1] and the standard model (SM) prediction of the muon anomalous magnetic moment $a_\mu = (g-2)_\mu/2$ triggers advents of the new measurements [2, 3] concurrent with progresses on the SM calculation. As the SM uncertainty is dominated by hadronic contributions in HVP and hadronic light-by-light (HLbL) scattering topologies, dedicated efforts have been put both into lattice QCD [4–13] and dispersion theory [14–23] beyond hadronic modelings.

The leading hadronic contribution, HVP, can be evaluated using $e^+e^- \to$ hadrons cross section data as input into a dispersion integral [24, 25]. Among the most recent data compilations of HVP [26–29], [26, 27] were performed following direct data-integration methods without additional model assumptions, where tensions between conflicting data sets are typically considered by a local error inflation. On the other hand, for low-multiplicity channels like 2π, a reconstruction of global fit functions from analyticity, unitarity, and low-energy theorems make it possible to confront the data with constraints from QCD. Such an investigation has been recently completed for the 2π channel below 1 GeV [30].

We analyze the 3π-channel contribution to HVP in the same vein, where the underlying hadronic input becomes the $\gamma^* \to 3\pi$ amplitude [31]. The final-state interactions between three pions are treated using the Khuri–Treiman equations, which were firstly applied to the $K \to 3\pi$ decay [32]. The $\gamma^* \to 3\pi$ amplitude plays a crucial role in the context of the pion-pole contribution to HLbL scattering [20, 21] and further enters as a left-hand cut in $\gamma^*\gamma^* \to \pi\pi$ [33–37]. For an isoscalar-photon virtuality $q^2 = M_\omega^2/M_\phi^2$, this amplitude is directly related to the three-particle decays of $\omega/\phi \to 3\pi$ [38–40].

2 HVP contribution to a_μ

The leading-order HVP contribution to a_μ reads [24, 25]

$$a_\mu = \Big(\frac{\alpha m_\mu}{3\pi}\Big)^2 \int_{s_\mathrm{thr}}^\infty \mathrm{d}s \frac{\hat{K}(s)}{s^2} R_\mathrm{had}(s), \tag{1}$$

where α is the fine-structure constant in the Thomson limit, and the kernel function is given by

$$\hat{K}(s) = \frac{3s}{m_\mu^2} \int_0^1 \mathrm{d}x \frac{x^2(1-x)}{x^2 + s/m_\mu^2(1-x)}. \tag{2}$$

$R_\mathrm{had}(s)$ is expressed in terms of the hadronic cross section as

$$R_\mathrm{had}(s) = \frac{3s}{4\pi\alpha^2} \sigma^0(e^+e^- \to \mathrm{hadrons}), \tag{3}$$

when the electron mass is neglected. Conventions need to be specified for the radiative corrections to the cross section so that higher-order insertions of HVP and HLbL scattering can be performed consistently [41–43]. In this regard, the "bare" cross section $\sigma^0(e^+e^- \to \mathrm{hadrons})$ should be inclusive of final-state radiation (FSR), but exempt from initial state radiation (ISR) and vacuum polarization (VP). As a consequence, s_thr is no longer equal to the two-pion threshold, but $s_\mathrm{thr} = M_{\pi^0}^2$ due to the $\pi^0\gamma$ channel.

[a] e-mail: longbai@hiskp.uni-bonn.de

Concerning the radiative corrections to the 3π channel, the ISR correction has usually been accounted for in the Monte Carlo generator of each experiment. We use the bare cross section provided by the experiment in which VP is already removed. Otherwise we uniformly apply the VP routine from [27]. We also constructed another VP function based on the 2π and 3π channels [30, 31] and conclude that the details of the VP routine prove irrelevant at the current level of precision. In the dispersive approach, the representation of the $\gamma^* \to 3\pi$ amplitude is only valid in pure QCD. Consequently, experimental data inclusive of FSR is incompatible with the dispersive treatment at first sight, because the photon contribution from FSR should be removed before the fit to extract quantities defined in pure QCD and added in a consistent perturbative manner afterwards. This strategy has been carried out in the 2π channel with the help of a scalar-QED approximation [30]. The HVP contribution of the 3π channel is more than one order of magnitude smaller. Hence, the total size of the $3\pi\gamma$ final-state contribution could be naively estimated as $\lesssim 0.3 \times 10^{-10}$, which is only borderline relevant at the present level of accuracy. Therefore, the FSR correction is neglected here and relegated to future work.

3 $\gamma^* \to 3\pi$ dispersive amplitude

We define the following matrix element of the electromagnetic current j_μ for the investigation of the $\gamma^* \to 3\pi$ amplitude

$$\begin{aligned}&\langle 0|j_\mu(0)|\pi^+(p_+)\pi^-(p_-)\pi^0(p_0)\rangle \\ &\quad = -\epsilon_{\mu\nu\rho\sigma}\, p_+^\nu p_-^\rho p_0^\sigma \mathcal{F}(s,t,u;q^2),\end{aligned} \tag{4}$$

where $q = p_+ + p_- + p_0$, $s = (q - p_0)^2$, $t = (q - p_+)^2$, $u = (q - p_-)^2$, and $s + t + u = 3M_\pi^2 + q^2$.

At low energy, the normalization of $\mathcal{F}$ is dictated by the Wess–Zumino–Witten (WZW) anomaly [44, 45] in the chiral limit [46–48],

$$\mathcal{F}(0,0,0;0) = \frac{1}{4\pi^2 F_\pi^3} \equiv F_{3\pi}, \tag{5}$$

where F_π is the pion decay constant. The s-channel partial-wave expansion of $\mathcal{F}$ reads [49]

$$\begin{aligned}\mathcal{F}(s,t,u;q^2) &= \sum_{l\ \mathrm{odd}} f_l(s,q^2) P_l'(\cos\theta_s), \\ \cos\theta_s &= \frac{t-u}{\sigma_\pi(s)\lambda^{1/2}(q^2,M_\pi^2,s)},\end{aligned} \tag{6}$$

with $\sigma_\pi(s) = \sqrt{1 - 4M_\pi^2/s}$, and $\lambda(a,b,c) = a^2 + b^2 + c^2 - 2(ab + ac + bc)$. The effects of higher partial waves beyond the P-wave are negligible below the $\rho_3(1690)$ resonance [31, 38, 50]. Accordingly, $\mathcal{F}$ can be decomposed into single-variable functions neglecting discontinuities of F- and higher partial waves,

$$\mathcal{F}(s,t,u;q^2) = \mathcal{F}(s,q^2) + \mathcal{F}(t,q^2) + \mathcal{F}(u,q^2). \tag{7}$$

At the same time, the discontinuity equation for the P-wave simplifies to

$$\mathrm{disc}\, f_1(s,q^2) = 2i\, f_1(s,q^2)\, \theta(s - 4M_\pi^2) \sin\delta(s)\, e^{-i\delta(s)}, \tag{8}$$

where $\delta(s)$ is the $\pi\pi$ P-wave phase shift. It gives a once-subtracted dispersive solution for $\mathcal{F}(s,q^2)$:

$$\mathcal{F}(s,q^2) = \Omega(s)\Big\{a(q^2) + \frac{s}{\pi}\int_{4M_\pi^2}^\infty \mathrm{d}s' \frac{\hat{\mathcal{F}}(s',q^2)\sin\delta(s')}{s'(s'-s)|\Omega(s')|}\Big\}, \tag{9}$$

where

$$\Omega(s) = \exp\left\{\frac{s}{\pi}\int_{4M_\pi^2}^\infty \mathrm{d}s' \frac{\delta(s')}{s'(s'-s)}\right\} \tag{10}$$

refers to the Omnès function [51] and $\hat{\mathcal{F}}$ contains the left-hand-cut contribution to the partial wave $f_1(s,q^2)$, see [21, 52, 53] for more details.

The iterative solution of the integral equation (9) is performed for $a(q^2) \to 1$, using the recently extracted phase shift $\delta(s)$ from [30] and a cutoff parameter $\Lambda_{3\pi} = 2.5\,\mathrm{GeV}$. Variations of $\delta(s)$ [54, 55] and $\Lambda_{3\pi}$ produce irrelevant systematic uncertainties compared to other sources.

The full $a(q^2)$ dependence in (9) can be restored as an overall normalization of the iterative solution and contains the information of the isoscalar-photon coupling to 3π. It is determined by the low-energy theorem (5) at $q^2 = 0$, and is accessible in $e^+e^- \to 3\pi$ in the decay region $q^2 > 9M_\pi^2$. We take the improved parameterization from [20, 21]:

$$a(q^2) = \alpha_A + \frac{q^2}{\pi}\int_{s_\mathrm{thr}}^\infty \mathrm{d}s' \frac{\mathrm{Im}\,\mathcal{A}(s')}{s'(s'-q^2)} + C_p(q^2), \tag{11}$$

in which the subtraction constant α_A is determined by the chiral anomaly (corrected by quark-mass renormalization) [56, 57],

$$\alpha_A = \frac{F_{3\pi}}{3} \times 1.066(10). \tag{12}$$

The function $\mathcal{A}$ is given by the sum of resonance contributions

$$\mathcal{A}(q^2) = \sum_V \frac{c_V}{M_V^2 - q^2 - i\sqrt{q^2}\,\Gamma_V(q^2)}, \tag{13}$$

with $V = \omega, \phi, \omega'(1420)$, and $\omega''(1650)$. The energy-dependent widths $\Gamma_{\omega/\phi}(q^2)$ of ω/ϕ include all the main decay channels, see [20, 21] for more details. For ω' and ω'', with masses and widths taken from the PDG [58], we assume a 100% branching ratio to 3π. We allow the masses and widths of ω and ϕ to vary: noticeable differences between the VP-subtracted parameters and the PDG are expected, since radiative effects are subsumed in the PDG parameters.

Non-resonant, inelastic effects are taken into account in (11) by the conformal polynomial

$$\begin{aligned}C_p(q^2) &= \sum_{i=1}^p c_i\big(z(q^2)^i - z(0)^i\big), \\ z(q^2) &= \frac{\sqrt{s_\mathrm{inel} - s_1} - \sqrt{s_\mathrm{inel} - q^2}}{\sqrt{s_\mathrm{inel} - s_1} + \sqrt{s_\mathrm{inel} - q^2}}.\end{aligned} \tag{14}$$

The inelastic threshold $s_\mathrm{inel} = 1\,\mathrm{GeV}^2$ is motivated by the nearby $K\bar{K}$ threshold, and the second parameter s_1 is set to $-1\,\mathrm{GeV}^2$. Further constraints are implemented to eliminate the S-wave cusp in the conformal polynomial (14)

and to ensure that the sum rule

$$\alpha_A = \frac{1}{\pi}\int_{s_{\rm thr}}^{\infty} \mathrm{d}s' \frac{\mathrm{Im}\,\mathcal{A}(s')}{s'} + \frac{1}{\pi}\int_{s_{\rm inel}}^{\infty} \mathrm{d}s' \frac{\mathrm{Im}\,C_p(s')}{s'} \quad (15)$$

is fulfilled exactly. Constructed in such a way, $a(q^2)$ thus obeys the low-energy theorem from the chiral anomaly, preserves analyticity of $\mathcal{F}(s,t,u;q^2)$, and is flexible enough to describe the data up to 1.8 GeV.

Finally, the relation between the bare cross section (neglecting the electron mass) and the scalar amplitude $\mathcal{F}(s,t,u;q^2)$ is given by

$$\sigma^0_{e^+e^-\to 3\pi}(q^2) = \alpha^2 \int_{s_{\rm min}}^{s_{\rm max}} \mathrm{d}s \int_{t_{\rm min}}^{t_{\rm max}} \mathrm{d}t\, \frac{\mathrm{d}^2\sigma}{\mathrm{d}s\,\mathrm{d}t}\,, \quad (16)$$

and

$$\frac{\mathrm{d}^2\sigma}{\mathrm{d}s\,\mathrm{d}t} = \frac{(s-4M_\pi^2)\,\lambda(q^2,M_\pi^2,s)\sin^2\theta_s}{768\,\pi\,q^6}\left|\mathcal{F}(s,t,u;q^2)\right|^2. \quad (17)$$

The integration boundaries are given as

$$s_{\rm min} = 4M_\pi^2, \qquad s_{\rm max} = (\sqrt{q^2}-M_\pi)^2,$$
$$t_{\rm min/max} = (E_-^* + E_0^*)^2 - \left(\sqrt{E_-^{*2}-M_\pi^2} \pm \sqrt{E_0^{*2}-M_\pi^2}\right)^2, \quad (18)$$

and

$$E_-^* = \frac{\sqrt{s}}{2}, \qquad E_0^* = \frac{q^2-s-M_\pi^2}{2\sqrt{s}}. \quad (19)$$

In the following we briefly discuss the data sets to which we perform our fit using (16) and (17).

4 Data sets and combined fits

We list the data sets which are included in our analysis in Table 1. The Novosibirsk experiments SND [59–62] and CMD-2 [63–66] provide the most precise measurements for the low-energy and ω- and ϕ-resonance regions. These data were obtained from direct energy scans. Only the BaBar experiment [70], which covers the higher-energy range above the ϕ, used the ISR technique. For completeness, we also take into account older data from DM1 [67], DM2 [68], and ND [69]. The statistical uncertainties of all data sets are given in diagonal form without further correlations. In contrast, the systematic uncertainties are divided into normalization uncertainties usually arising from luminosity measurement or detection efficiency, which are 100% correlated by definition, and other sources of systematic effects (for instance model assumptions and background) restricted to localized energy regions, which should not be considered correlated. We follow the experimental documentation to the best of our knowledge and consider a systematic error of normalization type whenever given as a percentage, and the remaining one as a diagonal error. Additionally, BaBar [70] explicitly states that the systematic errors of the data obtained by ISR for different energy bins are fully correlated.

It is well known that a normalization uncertainty may introduce a potential bias in the fit. More explicity, a χ^2-minimization with an empirical covariance matrix $\mathrm{V}(i,j)$ including a normalization uncertainty,

$$\chi^2 = \sum_{i,j}(f(x_i)-y_i)\mathrm{V}(i,j)^{-1}(f(x_j)-y_j), \quad (20)$$

will converge to a solution that is biased towards a lower value, as firstly observed by D'Agostini [71]. This bias can be severe for a large number of data points or large normalization uncertainties. We follow the iterative fit method proposed by the NNPDF collaboration [72] to eliminate the bias. To this end, the corrected iterative covariance matrix reads

$$\mathrm{V}_{n+1}(i,j) = \mathrm{V}^{\rm stat}(i,j) + \frac{\mathrm{V}^{\rm syst}(i,j)}{y_i y_j} f_n(x_i) f_n(x_j), \quad (21)$$

where $\mathrm{V}^{\rm stat}(i,j)$ is the statistical covariance matrix, and the systematic covariance matrix $\mathrm{V}^{\rm syst}(i,j)$ is determined by multiplying the normalization factors with the fit model in each iteration step. Rapid convergence to the final solution is expected after a few iteration steps.

Our combined fit results are shown in Table 2, where we apply $p_{\rm conf} = 2\ldots4$ free parameters in the conformal polynomial, added together with other dispersive uncertainties to estimate the systematic uncertainty of our analysis. We include the fits with diagonal errors and full ones simultaneously to better monitor the role of correlations, but use the latter as our final estimate. Combinations of different data sets reveal acceptable consistency and statistics except for [66], wherein the last few data points of each scan below 5 nb cause unacceptable χ^2 and the third scan produces a significantly lower ϕ mass. Accordingly, we have to remove the data with very small cross sections mentioned above and allow for a rescaling

$$\sqrt{s} \to \sqrt{s} + \xi(\sqrt{s} - 3M_\pi) \quad (22)$$

in the right ballpark with the energy-calibration uncertainties in the third scan data. In addition, we discard the DM2 data [68] since they disagree with both SND [62] and BaBar [70] high-statistics data.

Our central value is fixed by the best statistical fit with $p_{\rm conf} = 3$, as illustrated in the left plot of Figure 1. In particular, we find the vacuum-polarization-subtracted ω and ϕ parameters

$$\begin{aligned} M_\omega &= 782.63(3)(1)\,\mathrm{MeV} = 782.63(3)\,\mathrm{MeV},\\ \Gamma_\omega &= 8.71(4)(4)\,\mathrm{MeV} = 8.71(6)\,\mathrm{MeV},\\ M_\phi &= 1019.20(2)(1)\,\mathrm{MeV} = 1019.20(2)\,\mathrm{MeV},\\ \Gamma_\phi &= 4.23(4)(2)\,\mathrm{MeV} = 4.23(4)\,\mathrm{MeV}, \end{aligned} \quad (23)$$

where the fit errors are inflated by the scale factor

$$S = \sqrt{\chi^2/\mathrm{dof}}, \quad (24)$$

following the PDG prescription [58]. The differences to the PDG parameters can be traced back to the subtraction

Experiment	Region of $\sqrt{s}$ [GeV]	# data points	Normalization uncertainty
SND 2002 [59, 60]	[0.98, 1.38]	67	5.0% (data from [59]) 5.4% (otherwise)
SND 2003 [61]	[0.66, 0.97]	49	3.4% for $\sqrt{s} < 0.9\,\text{GeV}$ 4.5% for $\sqrt{s} > 0.9\,\text{GeV}$
SND 2015 [62]	[1.05, 1.80]	31	3.7%
CMD-2 1995 [63]	[0.99, 1.03]	16	4.6%
CMD-2 1998 [64]	[0.99, 1.03]	13	2.3%
CMD-2 2004 [65]	[0.76, 0.81]	13	1.3%
CMD-2 2006 [66]	[0.98, 1.06]	54	2.5%
DM1 1980 [67]	[0.75, 1.10]	26	3.2%
DM2 1992 [68]	[1.34, 1.80]	10	8.7%
ND 1991 [69]	[0.81, 1.39]	28	10% for $\sqrt{s} < 1.0\,\text{GeV}$ 20% for $\sqrt{s} > 1.0\,\text{GeV}$
BaBar 2004 [70]	[1.06, 1.80]	30	all systematics

Table 1. Summary table of $e^+e^- \to 3\pi$ data sets. Only data points below 1.8 GeV are included from [62, 68, 70]. In the last column, normalization-type systematic uncertainties are assumed to be 100% correlated.

of radiative effects, which reveals a perfect agreement between (23) and the PDG average [58] for the ϕ, with an anticipated downward shift of 0.26 MeV for the mass and negligible correction to the width. In view of a downward shift of 0.13 MeV and an upward shift of 0.06 MeV for the mass and width of the ω, this analysis solidifies the tension with the VP-subtracted ω mass extracted from the 2π channel [30].

5 Consequences for a_μ

We find our final result for the 3π contribution to a_μ to be

$$a_\mu^{3\pi}|_{\le 1.8\,\text{GeV}} = 46.2(6)(6) \times 10^{-10} = 46.2(8) \times 10^{-10}. \quad (25)$$

It is in very good agreement with $a_\mu^{3\pi}|_{\le 1.8\,\text{GeV}} = 46.2(1.5) \times 10^{-10}$ from [26], moreover, providing a reduced uncertainty. The deviation from [27] is mainly due to the different interpolation methods applied to the integration of the data: a linear interpolation reproduces the central value $a_\mu^{3\pi}|_{\le 1.8\,\text{GeV}} = 47.7(9) \times 10^{-10}$ from [27], while higher-order interpolations produce smaller values closer to (25).[1] Estimates as low as $a_\mu^{3\pi}|_{\le 2.0\,\text{GeV}} = 44.3(1.5) \times 10^{-10}$ [74] are not supported by our analysis. We find a larger contribution from the near threshold region, $a_\mu^{3\pi}|_{\le 0.66\,\text{GeV}} = 0.02 \times 10^{-10}$, twice as large as the value from [75]. The estimate of [75] follows the analyses [76, 77], which are based on a model with a contact term determined by the WZW anomaly and vector meson dominance. This model is depicted in the right plot of Figure 1, where it undershoots the lowest-energy data points.

We combine our result with the 2π channel from [30] and obtain the HVP contribution with analyticity and unitarity constraints imposed,

$$\begin{aligned} &a_\mu^{2\pi}|_{\le 1.0\,\text{GeV}} + a_\mu^{3\pi}|_{\le 1.8\,\text{GeV}} \\ &= [495.0(2.6) + 46.2(8)] \times 10^{-10} \\ &= 541.2(2.7) \times 10^{-10}, \end{aligned} \quad (26)$$

which covers nearly 80% of the total HVP integral. Adding the remaining HVP contributions from [26, 27], a conservative HLbL estimate $a_\mu^{\text{HLbL}} = 10(4) \times 10^{-10}$, QED [78], electroweak [79], and higher-order hadronic [27, 42, 43] contributions, we reaffirm the $(g-2)_\mu$ anomaly at the level of 3.4σ.

6 Conclusions and outlook

We have reported on a comprehensive dispersive analysis of the 3π contribution to HVP. We first constructed the $\gamma^* \to 3\pi$ amplitude imposing constraints from analyticity, unitarity, and the low-energy theorem of QCD. We performed the fit to the combined data sets using the aforementioned amplitude, and eliminated the potential bias related to the normalization uncertainties. After these setups, we were able to check the consistencies of different data sets. Identifying the tensions in [66], our analysis completes another independent check for the 3π-channel HVP contribution with the global fit function fulfilling QCD constraints, complementary to strategies based on direct integration of the data.

[1] This observation has lead to a modified integration of the data in the ω-peak region in the most recent update [73].

	diagonal			full		
$p_{\rm conf}$	2	3	4	2	3	4
χ^2/dof	361.3/306	354.6/305	354.0/304	443.7/306	430.8/305	430.7/304
	= 1.18	= 1.16	= 1.16	= 1.45	= 1.41	= 1.42
p-value	0.02	0.03	0.03	4×10^{-7}	3×10^{-6}	2×10^{-6}
M_ω [MeV]	782.60(4)	782.60(4)	782.60(4)	782.63(2)	782.63(2)	782.63(2)
Γ_ω [MeV]	8.75(6)	8.79(6)	8.77(6)	8.69(3)	8.71(3)	8.71(3)
M_ϕ [MeV]	1019.23(2)	1019.22(2)	1019.22(2)	1019.20(1)	1019.20(1)	1019.20(1)
Γ_ϕ [MeV]	4.34(4)	4.32(4)	4.32(4)	4.24(3)	4.23(3)	4.23(3)
c_ω [GeV^{-1}]	2.87(1)	2.89(1)	2.88(1)	2.85(2)	2.86(2)	2.86(2)
c_ϕ [GeV^{-1}]	−0.395(3)	−0.394(3)	−0.394(3)	−0.388(3)	−0.386(3)	−0.386(3)
$c_{\omega'}$ [GeV^{-1}]	−0.18(3)	−0.09(5)	−0.08(5)	−0.17(3)	−0.07(4)	−0.06(4)
$c_{\omega''}$ [GeV^{-1}]	−1.65(8)	−1.52(10)	−1.55(10)	−1.65(8)	−1.52(8)	−1.53(10)
c_1 [GeV^{-3}]	−0.35(10)	−0.22(11)	−0.24(11)	−0.31(10)	−0.12(11)	−0.14(12)
c_2 [GeV^{-3}]	−1.28(4)	−1.39(6)	−1.33(9)	−1.24(4)	−1.36(5)	−1.34(9)
c_3 [GeV^{-3}]	—	−0.48(8)	−0.51(9)	—	−0.47(7)	−0.48(8)
c_4 [GeV^{-3}]	—	—	1.39(9)	—	—	1.41(9)
$10^4 \times \xi$	1.9(7)	1.8(7)	1.8(7)	1.3(5)	1.3(5)	1.3(5)
$10^{10} \times a_\mu^{3\pi}\vert_{\le 1.8\,\rm GeV}$	46.65(21)	46.70(21)	46.67(22)	45.87(47)	46.16(47)	46.10(50)

Table 2. Fits to the combined data sets as shown in Table 1, with fit uncertainties given in brackets.

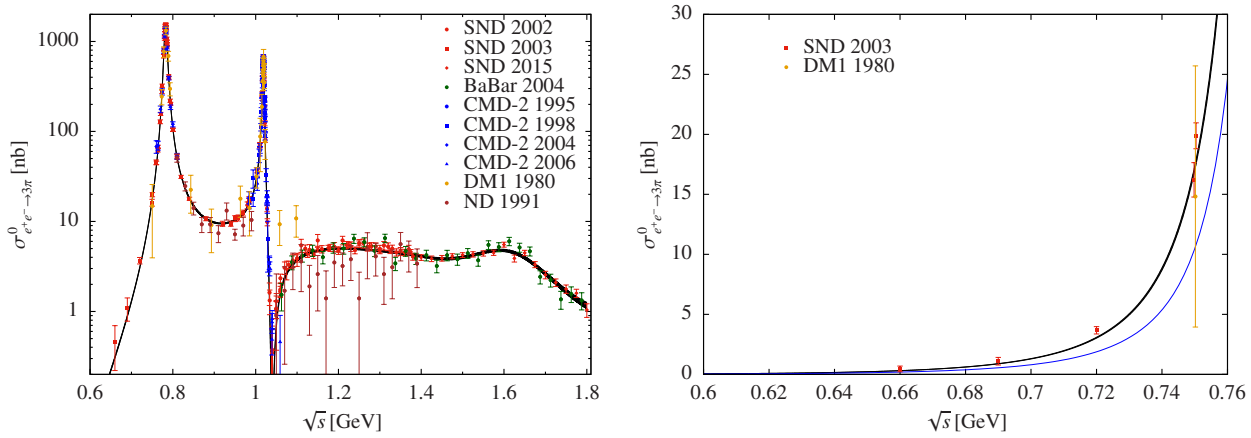

Figure 1. Fit to the bare $e^+e^- \to 3\pi$ data sets as listed in Table 1 (left) and the comparison to the estimate from [76, 77] (blue curve) in the near threshold region (right). The black error band represents the fit uncertainty.

We extracted the masses and widths of the ω and ϕ from our central fit and raised the potential impacts of radiative effects. The tension between the ω mass extracted from the 2π and 3π channels survives. Furthermore, our result of the 3π-channel contribution to a_μ scrutinized the discrepancies standing in the literature before. Detailed analysis of FSR is in progress and further improvements are expected in light of new data inputs.

Acknowledgment

We acknowledge Janak Prabhu for providing a cross-check for the model calculation based on [76, 77]. B.-L. H. is grateful to the organizers for the wonderful FCCP2019 workshop and Massimo Passera for the cordial invitation. Financial support by the DFG (CRC 110, “Symmetries and the Emergence of Structure in QCD”) and the DOE (Grant No. DE-FG02-00ER41132) is gratefully acknowledged.

References

[1] G. W. Bennett *et al.* [Muon $g-2$ Collaboration], Phys. Rev. D **73** (2006) 072003 [hep-ex/0602035].
[2] J. Grange *et al.* [Muon $g-2$ Collaboration], arXiv:1501.06858 [physics.ins-det].
[3] M. Abe *et al.*, PTEP **2019** (2019) 053C02 [arXiv:1901.03047 [physics.ins-det]].
[4] T. Blum, N. Christ, M. Hayakawa, T. Izubuchi, L. Jin, C. Jung and C. Lehner, Phys. Rev. Lett. **118** (2017) 022005 [arXiv:1610.04603 [hep-lat]].
[5] T. Blum, N. Christ, M. Hayakawa, T. Izubuchi, L. Jin, C. Jung and C. Lehner, Phys. Rev. D **96** (2017) 034515 [arXiv:1705.01067 [hep-lat]].
[6] S. Borsanyi *et al.* [BMW Collaboration], Phys. Rev. Lett. **121** (2018) 022002 [arXiv:1711.04980 [hep-lat]].
[7] T. Blum *et al.* [RBC and UKQCD Collaborations], Phys. Rev. Lett. **121** (2018) 022003 [arXiv:1801.07224 [hep-lat]].
[8] D. Giusti, F. Sanfilippo and S. Simula, Phys. Rev. D **98** (2018) 114504 [arXiv:1808.00887 [hep-lat]].
[9] E. Shintani and Y. Kuramashi [PACS Collaboration], Phys. Rev. D **100** (2019) 034517 [arXiv:1902.00885 [hep-lat]].
[10] C. T. H. Davies *et al.* [Fermilab Lattice and LATTICE-HPQCD and MILC Collaborations], arXiv:1902.04223 [hep-lat].
[11] A. Gérardin, H. B. Meyer and A. Nyffeler, Phys. Rev. D **100** (2019) 034520 [arXiv:1903.09471 [hep-lat]].
[12] A. Gérardin *et al.*, Phys. Rev. D **100** (2019) 014510 [arXiv:1904.03120 [hep-lat]].
[13] C. Aubin, T. Blum, C. Tu, M. Golterman, C. Jung and S. Peris, arXiv:1905.09307 [hep-lat].
[14] M. Hoferichter, G. Colangelo, M. Procura and P. Stoffer, Int. J. Mod. Phys. Conf. Ser. **35** (2014) 1460400 [arXiv:1309.6877 [hep-ph]].
[15] G. Colangelo, M. Hoferichter, M. Procura and P. Stoffer, JHEP **1409** (2014) 091 [arXiv:1402.7081 [hep-ph]].
[16] G. Colangelo, M. Hoferichter, B. Kubis, M. Procura and P. Stoffer, Phys. Lett. B **738** (2014) 6 [arXiv:1408.2517 [hep-ph]].
[17] G. Colangelo, M. Hoferichter, M. Procura and P. Stoffer, JHEP **1509** (2015) 074 [arXiv:1506.01386 [hep-ph]].
[18] G. Colangelo, M. Hoferichter, M. Procura and P. Stoffer, Phys. Rev. Lett. **118** (2017) 232001 [arXiv:1701.06554 [hep-ph]].
[19] G. Colangelo, M. Hoferichter, M. Procura and P. Stoffer, JHEP **1704** (2017) 161 [arXiv:1702.07347 [hep-ph]].
[20] M. Hoferichter, B.-L. Hoid, B. Kubis, S. Leupold and S. P. Schneider, Phys. Rev. Lett. **121** (2018) 112002 [arXiv:1805.01471 [hep-ph]].
[21] M. Hoferichter, B. L. Hoid, B. Kubis, S. Leupold and S. P. Schneider, JHEP **1810** (2018) 141 [arXiv:1808.04823 [hep-ph]].
[22] G. Colangelo, F. Hagelstein, M. Hoferichter, L. Laub and P. Stoffer, arXiv:1910.11881 [hep-ph].
[23] G. Colangelo, F. Hagelstein, M. Hoferichter, L. Laub and P. Stoffer, arXiv:1910.13432 [hep-ph].
[24] C. Bouchiat and L. Michel, J. Phys. Radium **22** (1961) 121.
[25] S. J. Brodsky and E. de Rafael, Phys. Rev. **168** (1968) 1620.
[26] M. Davier, A. Hoecker, B. Malaescu and Z. Zhang, Eur. Phys. J. C **77** (2017) 827 [arXiv:1706.09436 [hep-ph]].
[27] A. Keshavarzi, D. Nomura and T. Teubner, Phys. Rev. D **97** (2018) 114025 [arXiv:1802.02995 [hep-ph]].
[28] F. Jegerlehner, EPJ Web Conf. **199** (2019) 01010 [arXiv:1809.07413 [hep-ph]].
[29] M. Benayoun, L. Delbuono and F. Jegerlehner, arXiv:1903.11034 [hep-ph].
[30] G. Colangelo, M. Hoferichter and P. Stoffer, JHEP **1902** (2019) 006 [arXiv:1810.00007 [hep-ph]].
[31] M. Hoferichter, B. L. Hoid and B. Kubis, JHEP **1908** (2019) 137 [arXiv:1907.01556 [hep-ph]].
[32] N. N. Khuri and S. B. Treiman, Phys. Rev. **119** (1960) 1115.
[33] R. García-Martín and B. Moussallam, Eur. Phys. J. C **70** (2010) 155 [arXiv:1006.5373 [hep-ph]].
[34] M. Hoferichter, D. R. Phillips and C. Schat, Eur. Phys. J. C **71** (2011) 1743 [arXiv:1106.4147 [hep-ph]].
[35] B. Moussallam, Eur. Phys. J. C **73** (2013) 2539 [arXiv:1305.3143 [hep-ph]].
[36] I. Danilkin and M. Vanderhaeghen, Phys. Lett. B **789** (2019) 366 [arXiv:1810.03669 [hep-ph]].
[37] M. Hoferichter and P. Stoffer, JHEP **1907** (2019) 073 [arXiv:1905.13198 [hep-ph]].
[38] F. Niecknig, B. Kubis and S. P. Schneider, Eur. Phys. J. C **72** (2012) 2014 [arXiv:1203.2501 [hep-ph]].
[39] I. V. Danilkin, C. Fernández-Ramírez, P. Guo, V. Mathieu, D. Schott, M. Shi and A. P. Szczepaniak, Phys. Rev. D **91** (2015) 094029 [arXiv:1409.7708 [hep-ph]].
[40] M. Dax, T. Isken and B. Kubis, Eur. Phys. J. C **78** (2018) 859 [arXiv:1808.08957 [hep-ph]].
[41] J. Calmet, S. Narison, M. Perrottet and E. de Rafael, Phys. Lett. **61B** (1976) 283.
[42] A. Kurz, T. Liu, P. Marquard and M. Steinhauser, Phys. Lett. B **734** (2014) 144 [arXiv:1403.6400 [hep-ph]].
[43] G. Colangelo, M. Hoferichter, A. Nyffeler, M. Passera and P. Stoffer, Phys. Lett. B **735** (2014) 90 [arXiv:1403.7512 [hep-ph]].
[44] J. Wess and B. Zumino, Phys. Lett. **37B** (1971) 95.
[45] E. Witten, Nucl. Phys. B **223** (1983) 422.
[46] S. L. Adler, B. W. Lee, S. B. Treiman and A. Zee, Phys. Rev. D **4** (1971) 3497.
[47] M. V. Terent'ev, Phys. Lett. **38B** (1972) 419.
[48] R. Aviv and A. Zee, Phys. Rev. D **5** (1972) 2372.

[49] M. Jacob and G. C. Wick, Annals Phys. **7** (1959) 404 [Annals Phys. **281** (2000) 774].
[50] M. Hoferichter, B. Kubis and M. Zanke, Phys. Rev. D **96** (2017) 114016 [arXiv:1710.00824 [hep-ph]].
[51] R. Omnès, Nuovo Cim. **8** (1958) 316.
[52] S. P. Schneider, B. Kubis and F. Niecknig, Phys. Rev. D **86** (2012) 054013 [arXiv:1206.3098 [hep-ph]].
[53] M. Hoferichter, B. Kubis, S. Leupold, F. Niecknig and S. P. Schneider, Eur. Phys. J. C **74** (2014) 3180 [arXiv:1410.4691 [hep-ph]].
[54] R. García-Martín, R. Kamiński, J. R. Peláez, J. Ruiz de Elvira and F. J. Ynduráin, Phys. Rev. D **83** (2011) 074004 [arXiv:1102.2183 [hep-ph]].
[55] I. Caprini, G. Colangelo and H. Leutwyler, Eur. Phys. J. C **72** (2012) 1860 [arXiv:1111.7160 [hep-ph]].
[56] J. Bijnens, A. Bramon and F. Cornet, Phys. Lett. B **237** (1990) 488.
[57] M. Hoferichter, B. Kubis and D. Sakkas, Phys. Rev. D **86** (2012) 116009 [arXiv:1210.6793 [hep-ph]].
[58] M. Tanabashi *et al.* [Particle Data Group], Phys. Rev. D **98** (2018) 030001.
[59] M. N. Achasov *et al.*, Phys. Rev. D **63** (2001) 072002 doi:10.1103/PhysRevD.63.072002 [hep-ex/0009036].
[60] M. N. Achasov *et al.*, Phys. Rev. D **66** (2002) 032001 [hep-ex/0201040].
[61] M. N. Achasov *et al.*, Phys. Rev. D **68** (2003) 052006 [hep-ex/0305049].
[62] V. M. Aul'chenko *et al.*, J. Exp. Theor. Phys. **121** (2015) 27 [Zh. Eksp. Teor. Fiz. **148** (2015) 34].
[63] R. R. Akhmetshin *et al.*, Phys. Lett. B **364** (1995) 199.
[64] R. R. Akhmetshin *et al.*, Phys. Lett. B **434** (1998) 426.
[65] R. R. Akhmetshin *et al.* [CMD-2 Collaboration], Phys. Lett. B **578** (2004) 285 [hep-ex/0308008].
[66] R. R. Akhmetshin *et al.*, Phys. Lett. B **642** (2006) 203.
[67] A. Cordier *et al.*, Nucl. Phys. B **172** (1980) 13.
[68] A. Antonelli *et al.* [DM2 Collaboration], Z. Phys. C **56** (1992) 15.
[69] S. I. Dolinsky *et al.*, Phys. Rept. **202** (1991) 99.
[70] B. Aubert *et al.* [BaBar Collaboration], Phys. Rev. D **70** (2004) 072004 [hep-ex/0408078].
[71] G. D'Agostini, Nucl. Instrum. Meth. A **346** (1994) 306.
[72] R. D. Ball *et al.* [NNPDF Collaboration], JHEP **1005** (2010) 075 [arXiv:0912.2276 [hep-ph]].
[73] A. Keshavarzi, D. Nomura and T. Teubner, arXiv:1911.00367 [hep-ph].
[74] F. Jegerlehner, Springer Tracts Mod. Phys. **274** (2017) 1.
[75] K. Hagiwara, A. D. Martin, D. Nomura and T. Teubner, Phys. Rev. D **69** (2004) 093003 [hep-ph/0312250].
[76] E. A. Kuraev and Z. K. Silagadze, Phys. Atom. Nucl. **58** (1995) 1589 [Yad. Fiz. **58N9** (1995) 1687] [hep-ph/9502406].
[77] A. I. Ahmedov, G. V. Fedotovich, E. A. Kuraev and Z. K. Silagadze, JHEP **0209** (2002) 008 [Phys. Atom. Nucl. **67** (2004) 985] [Yad. Fiz. **67** (2004) 1006] [hep-ph/0201157].
[78] T. Aoyama, T. Kinoshita and M. Nio, Phys. Rev. D **97** (2018) 036001 [arXiv:1712.06060 [hep-ph]].
[79] C. Gnendiger, D. Stöckinger and H. Stöckinger-Kim, Phys. Rev. D **88** (2013) 053005 [arXiv:1306.5546 [hep-ph]].